Respiratory Research

RESEARCH

Open Access

Intrapleural dual blockade of IL-6 and PD-L1 reprograms CAF dynamics and the tumor microenvironment in lung cancer-associated malignant pleural effusion

Qinpei Cheng[1†], Xueying Zuo[1†], Zimu Wang[1,2], Wanjun Lu[1], Yuxin Jiang[3], Jiaxin Liu[1,2], Xinying Li[1,2], Qiuli Xu[3], Suhua Zhu[1], Xin Liu[1], Yong Song[1,3*], Ping Zhan[1*] and Tangfeng Lv[1,3*]

Abstract

Background Malignant pleural effusion (MPE) is a severe complication in lung cancer, characterized by an immunosuppressive tumor microenvironment (TME) and limited therapeutic options. This study investigates the role of IL-6 in regulating immune suppression and tumor progression in MPE and evaluates the efficacy of dual IL-6 and PD-L1 blockade.

Methods IL-6 levels were measured in MPE and paired serum samples from lung cancer patients, and correlations with PD-L1 expression and clinical outcomes were analyzed using publicly available datasets. RNA sequencing and immune deconvolution were used to assess immune cell infiltration. CAFs and immune cell infiltration were further evaluated using flow cytometry, immunohistochemistry, and multiplex immunofluorescence. In vitro co-culture systems were employed to simulate the MPE microenvironment and explore IL-6 interactions with CAFs, as well as its regulatory effect on tumor cell PD-L1 expression.

Results IL-6 levels were significantly elevated in MPE compared to paired serum and correlated with higher PD-L1 expression and poor survival outcomes in lung cancer patients. In the MPE mouse model, combination therapy with IL-6 and PD-L1 blockade reduced MPE volume, tumor burden, and PD-L1 expression, while enhancing T cell infiltration and alleviating TME immunosuppression. IL-6 was found to drive a positive feedback loop with iCAFs, promoting an immunosuppressive environment. In vitro, IL-6 from the MPE upregulated tumor cell PD-L1 expression the IL-6/STAT3 pathway.

Conclusion This study identifies IL-6 as a critical contributor of immune suppression and tumor progression in MPE. The combination of IL-6 and PD-L1 blockade effectively alleviated immunosuppression and reduced tumor burden, offering a potential therapeutic approach for MPE management.

Keywords Malignant pleural effusion, Lung cancer, IL-6, PD-L1, Cancer-associated fibroblast, Immunotherapy

[†]Qinpei Cheng and Xueying Zuo contributed equally to this work.

*Correspondence:
Yong Song
yong.song@nju.edu.cn
Ping Zhan
zhanping207@163.com
Tangfeng Lv
TangfengLv7210@nju.edu.cn
Full list of author information is available at the end of the article

© The Author(s) 2025. **Open Access** This article is licensed under a Creative Commons Attribution-NonCommercial-NoDerivatives 4.0 International License, which permits any non-commercial use, sharing, distribution and reproduction in any medium or format, as long as you give appropriate credit to the original author(s) and the source, provide a link to the Creative Commons licence, and indicate if you modified the licensed material. You do not have permission under this licence to share adapted material derived from this article or parts of it. The images or other third party material in this article are included in the article's Creative Commons licence, unless indicated otherwise in a credit line to the material. If material is not included in the article's Creative Commons licence and your intended use is not permitted by statutory regulation or exceeds the permitted use, you will need to obtain permission directly from the copyright holder. To view a copy of this licence, visit http://creativecommons.org/licenses/by-nc-nd/4.0/.

Introduction

Malignant pleural effusion (MPE), a severe complication in cancer, is predominantly caused by metastatic tumors like lung cancer [1], which leads to a poor prognosis with a median survival of less than a year [2]. Despite advancements in cancer therapies, current treatments for MPE remains largely palliative [3]. MPE arises from various factors, including disruption lymphatic drainage, increased capillary and pleural permeability, elevated fluid production [4]. This results in the accumulation of exudative effusion rich in tumor and immune cells [5], which fosters a pro-tumorigenic and immunosuppressive microenvironment featuring hypoxia and immune evasion [6]. Recent advances in immune checkpoint blockade (ICB) have shown significant benefits [7, 8]. However, resistance remains a critical challenge [9], particularly in MPE and other "cold" tumors, which underscores the need for novel therapeutic strategies [10].

Interleukin-6 (IL-6) as a cytokine prevalent in the tumor microenvironment (TME) of MPE has been implicated in tumor progression and the suppression of immune responses [11]. Elevated IL-6 levels are frequently observed in various cancers, including lung cancer, where it promotes tumor progression through the IL-6/STAT3 signaling pathway [12, 13]. It is produced by tumor-associated macrophages (TAMs), tumor cells, cancer-associated fibroblasts (CAFs), $CD4^+$ T cells, myeloid-derived suppressor cells (MDSCs), and other cells [12, 14, 15]. A major source of IL-6 in MPE is pleural mesothelial cells (PMCs) [16], which can transition into myofibroblasts via mesothelial-to-mesenchyme transition (MMT) [17, 18]. These cells contribute to the immunosuppressive microenvironment and facilitate the immune evasion of tumor cells partly through the upregulation of immune checkpoints [13]. Recent preclinical studies have shown that the inhibition of IL-6 combined with the blockade of programmed cell death protein 1 (PD-1)/programmed cell death protein 1 ligand 1 (PD-L1) has the potential to improve tumor control. Nevertheless, their potential interaction and combined impact on MPE remain unclear [19–23].

CAFs are a critical component of the TME and are increasingly recognized for their functional heterogeneity [24–26]. Distinct CAF subtypes, such as inflammatory CAFs (iCAFs) and myofibroblastic CAFs (myCAFs), exhibit divergent roles in tumor progression [27]. There is ongoing debate over the role of myCAFs, with conflicting evidence about pro-tumorigenic or suppressive effects in different tumors [28–30]. Considering that myCAFs and iCAFs are known for their interconversion capabilities influenced by tumor-derived signals [31], targeting specific signaling molecules and pathways rather than specific CAF subtype may be a more viable therapeutic strategy [32]. Despite the differences across cancer types, the IL-6/IL-6 receptor (IL-6R) signaling emerges as a consistent pro-tumorigenic hallmark of iCAFs [32]. These CAFs generally associated with an immunosuppressive environment owing to high cytokine expression and low extracellular matrix (ECM) production [33] represent a critical target for enhancing ICB therapy [34]. Therefore, anti-IL-6 therapies like tocilizumab are expected to target these CAFs and be therapeutically beneficial [15, 35–37]. However, the role of CAFs in the TME, particularly in MPE, remains underexplored.

This study aims to address these gaps by investigating the therapeutic potential of dual blockade of IL-6 and PD-L1 in MPE. We comprehensively analyze the effects of this combination therapy on the TME, with a particular focus on its impact on CAF subtypes and the IL-6/STAT3 signaling pathway. Our findings provide critical insights into the molecular interplay within the MPE microenvironment and highlight the therapeutic potential of targeting both IL-6 and PD-L1.

Materials and methods

Cells and cell culture

Lewis lung carcinoma (LLC) and the National Institutes of Health (NIH)/3T3 cells were supplied by the Shanghai Cell Bank of the Chinese Academy of Sciences (Shanghai, China). LLC-luciferase (LUC) was generated from LLC stably transfected with a lentivirus carrying the luciferase vector (GV260, Genechem, Shanghai, China) and selected by 4 μg/mL puromycin (Beyotime, Shanghai, China). LLC, NIH/3T3 and LLC-LUC cells were all cultured in Dulbecco's modified Eagle medium (DMEM, Gibco, USA) with 10% fetal bovine serum (FBS, Gibco, USA). Human NSCLC cells (A549) offered by the Shanghai Cell Bank of Chinese Academy of Sciences were cultured in Ham's F-12K (F-12K, Meilunbio, Dalian, China) with 10% FBS. After being authenticated by the analysis of short tandem repeats, LLC and A549 cell lines were tested negative for mycoplasma contamination within the last six months and utilized at passage numbers < 10.

Primary lung CAFs and normal fibroblasts (NFs) were extracted from lung cancer tissues and counterpart normal lung tissues, which were acquired from two patients diagnosed with lung cancer in this institution. Tissues were chopped and digested with 1 mg/ml collagenase type IV (C5138, Sigma-Aldrich, USA) at 37 ℃ for 1 h to isolate CAFs and NFs. Obtained with proper informed consent from the patients, all specimens gained the approval of the Ethical Committee and Institutional Review Board of Jinling Hospital. The culturing of CAFs and NFs was completed with DMEM/Nutrient Mixture F-12 (DMEM/F-12, Gibco, USA) containing 10%−20% FBS.

Peripheral blood mononuclear cells (PBMCs) were separated from 10 ml of peripheral blood obtained from healthy donors with informed consent. Collected blood was diluted with an equivalent volume of phosphate buffered saline (PBS) and received 15-min centrifugation with Ficoll density gradient centrifugation (Solarbio, Beijing, China) in a SepMate PBMC isolation tube (Stemcell, USA) at 400 g at room temperature. A red blood cell (RBC) lysis solution (Biolegend, USA) was employed to lyse residual red blood cells, and PBMCs were rinsed twice with PBS. Subsequently, these cells were counted and used immediately for indirect co-culture with CAFs at a ratio of 5:1 with a transwell system (Labselect, Hefei, China). CAFs were serum-starved for 12 h before treatment.

All cell culture medium was supplemented with penicillin (100 U/mL) streptomycin (100 mg/mL). All cells were maintained at 37 ℃ in a humidified atmosphere with 5% carbon dioxide (CO_2). For in vitro conditions, the following reagents were used: recombinant human IL-6 protein (206-IL-010, R&D Systems, USA), S3I-201 (S1155, Selleck Chemicals, USA), and tocilizumab (Roche, Switzerland).

Mice and MPE models

Male C57BL/6J mice aged six weeks were bought from the Model Animal Research Center of Nanjing University (Nanjing, China). The MPE mouse model was prepared by an intrapleural injection of 5×10^5 LLC or LLC-LUC cells [8] (Supplementary Figs. 1A-C). Mice were randomly divided into four groups: Vehicle, anti-IL-6 monoclonal antibody (mAb), anti-PD-L1 monoclonal antibody (mAb), as well as anti-IL-6 mAb and anti-PD-L1 mAb groups. Mice were intrapleurally injected with 200 μg anti-PD-L1 mAb (Clone:10F.9G20, BE0101, BioXcell, USA) and/or anti-IL-6 mAb (Clone: MP5-20F3, BE0046, BioXcell, USA) or IgG2b isotype control (Clone: LTF-2, BE0090, BioXcell, USA) on the 7th and 14th days of the model, following dosages used in previous studies [19–21] and in our earlier optimization experiments on MPE models [8]. For the MPE model injected with LLC-LUC cells, the observation of mice was performed by bioluminescence imaging on the 7th and 14th days before intrapleural injection and the 21st day before scarification. MPE specimens and tumor nodules were collected and measured on the 21st day. The survival status of MPE mice was observed every day until a fatal outcome for all mice.

To evaluate the function of CAFs, the mice were intrapleurally injected with either 5×10^5 LLC/LLC-LUC cells only or 5×10^5 LLC/LLC-LUC and 1×10^6 NIH/3T3 cells [35]. To investigate the synergistic effects of IL-6 inhibitor and PD-L1 blockade, the mice injected with LLC/LLC-LUC and NIH/3T3 cells were administered with 200 μg anti-IL-6 mAb and 200 μg anti-PD-L1 mAb on the 7th and 14th days.

Bioluminescence imaging

MPE mice were anesthetized by use of 2.5% isoflurane with a constant flow for anesthesia maintenance. Then, mice received an intraperitoneal injection of 200 μl D-luciferin (UElandy, 15 mg/ml in PBS, Suzhou, China). After 10 min, they were placed within the chamber of the IVIS Lumina XR system (PerkinElmer) for imaging. Imaging sessions were scheduled on days 7, 14 and 21 after cell inoculation. Images were obtained with an exposure time of 1 min. The bioluminescence signal was quantified as total photon flux. The total photon flux from luminescent images was analyzed using the dedicated software provided by the IVIS Lumina XR system.

Patients and MPE collection

A total of 26 MPE specimens were gathered from patients diagnosed with lung cancer at the Department of Respiratory and Critical Care Medicine of Jinling Hospital of Medical School of Nanjing University (Nanjing, China) between October 2020 and November 2022. Every specimen was obtained with proper informed consent from the patients and gained the approval of the Ethical Committee and Institutional Review Board of Jinling Hospital. Clinicopathological information is presented in Supplementary Table 1.

Sample processing and enzyme-linked immunosorbent assay

Human and mouse samples including peripheral blood and pleural effusion were initially centrifuged at 3,000 rpm at 4 °C for 15 min after collection. Afterwards, supernatants were meticulously aliquoted and stored at −80 °C until their analysis. The culture media from cell co-culture systems was filtered through a 0.22-μm filter (Merck, German) after collection and kept at −80 °C. The levels of IL-6 (Novus Biologicals, USA) in the above samples were determined as per the instructions of the manufacturer.

Isolation of cells from mouse tumor nodules

Mouse tumor tissues were minced into 1 mm^3 pieces and enzymatically dissociated in a digestion mix with 125 μg/ml Liberase TL (5401020001, Roche, Switzerland) and 100 U/ml DNase I (10104159001, Roche, Switzerland) at 37 °C for 60 min. The digestion process was terminated by adding DMEM with 10% FBS. The cell suspension was obtained by straining through a 70 μm cell strainers (Falcon, USA). Next, the single-cell suspension was lysed with an RBC lysis solution and then rinsed with PBS,

followed by the counting and resuspension of cells in a staining buffer.

Flow cytometry

After being resuspended in a staining buffer, the cells were incubated with an Fc blocking reagent (553141, BD, USA) for 10 min. After that, surface antibodies were added and stained for 30 min at the temperature of 4 °C in the dark. Then, the cells were permeabilized for 45 min by a transfascial (TF) fixation/permeabilization working solution (562574, BD, USA) at 4 °C in the dark, and rinsed twice with diluted 1× permeabilization/wash buffer. Next, intracellular antibodies were added and stained for 30 min at the temperature of 4 °C in the dark. After staining, cells were washed and analyzed by BD FACSCantoII flow cytometer (BD). FlowJo software was used for data analysis. Antibodies used are listed in Supplementary Table 2, and the panels are presented in Supplementary Table 3.

Hematoxylin and eosin staining, immunohistochemistry, and multiplex immunofluorescence

Mouse pleural and tumor nodules were fixed, embedded in paraffin, and sectioned. For hematoxylin and eosin (H&E) staining, sections were deparaffinized, rehydrated and stained with hematoxylin to color nuclei blue and eosin for cytoplasmic pink staining, followed by dehydration and mounting. For the immunohistochemistry (IHC) of tumor nodules, sections were treated with hydrogen peroxide to block endogenous peroxidase activity after a similar preparation of deparaffinization and rehydration. Then, antigens were retrieved using either sodium citrate (pH 6.0, MXB, Fuzhou, China) or 2-Amino-2-(hydroxymethyl)-1,3-propanediol-ethylene diamine tetraacetic acid (Tris-EDTA) buffer (pH 9.0, Servicebio, Wuhan, China) depending on antibodies by heating the sections at 95 ℃ for 10 min. After 1-h blockade with 5% goat serum at room temperature, sections were incubated with primary antibody at 4 ℃ for one night. Antibodies used were as follows: alpha-smooth muscle actin (α-SMA, ab124964, Abcam, 1:2000), fibroblast activation protein (FAP, ab240989, Abcam, 1:100), IL-6 (ab290735, Abcam, 1:100), CD4 (#25229, CST, 1:200), CD8 (#98941, CST, 1:500), phosphorylated signal transducer and activator of transcription 3 (p-STAT3, Tyr705, #9145, CST, 1:250), F4/80 (#70076, CST, 1:500), forkhead box protein P3 (FOXP3, bs-10211R, Bioss, 1:300), podoplanin (A21748, Abclonal, 1:200) and platelet derived growth factor receptor alpha (PDGFRα, A2103, Abclonal, 1:200). After washing, sections were incubated with horseradish peroxidase (HRP)-conjugated secondary antibodies at room temperature for 1 h. The expression of the indicated protein was visualized by diaminobenzidine (DAB, Abcam) and counterstained with hematoxylin. Then, sections were dehydrated and mounted.

Multiplex immunofluorescence by tyramide signal amplification (TSA) assays (Runnerbio, Shanghai, China) aimed to explore the expression of iCAFs in mouse tumor nodules. The sequence of staining was PDGFRα-Try-488, IL-6-Try-cy3, FAP-Try-594, and α-SMA-Try-cy5. Samples were covered with an anti-fade mounting medium containing 4,6-diamino-2-phenyl indole (DAPI, Beyotime, Shanghai, China) and captured using the digital slide scanner Pannoramic SCAN II(3DHISTECH, Hungary).

Immunofluorescence

After being fixed with 4% paraformaldehyde, CAFs and NFs were both permeabilized with Triton X-100 and blocked with bovine serum albumin (BSA). The following primary antibodies were used to incubate cells at 4 °C overnight: α-SMA (ab7817, Abcam, 1:1000) and FAP (ab240989, Abcam, 1:100). After being washed, cells underwent incubation with Alexa Fluor 594-conjugated anti-rabbit secondary antibodies for FAP and Alexa Fluor 488-conjugated anti-mouse secondary antibodies for α-SMA, and then counterstaining with DAPI. A fluorescence microscope (Zeiss) was utilized to detect fluorescence signals.

RNA isolation and sequencing

The total RNA of homogenized mouse pleural tissues containing tumor nodules was extracted using TRIzol (Takara), and its quality was verified by the use of an Agilent 2100 Bioanalyzer. Then, messenger RNA (mRNA) was enriched, fragmented and reverse transcribed into

(See figure on next page.)

Fig. 1 Synergistic effects of IL-6 inhibition combined with PD-L1 blockade in the MPE mouse model. **A** Schematic representation of the treatment protocol, including the timing of administration and duration of treatments for the anti-IL-6 mAb (200 μg), anti-PD-L1 mAb (200 μg), their combination, and the vehicle solution in the MPE mouse model. The MPE mice were randomly assigned to four treatment groups. Created with BioRender. **B** Representative in vivo bioluminescence images of the growth of mice MPE. **C** MPE volume, **D** tumor nodules numbers, **E** representative images of tumors, **F** Kaplan–Meier survival plot, **G** body weight, levels of **H** ALT, **I** AST, **J** Cre in the blood was observed. **K** Representative H&E staining images of pleural tissue sections Scale bar = 100 μm. All experiments were performed with ≥ 3 biological replicates. *$P < 0.05$, **$p < 0.01$, ***$p < 0.001$, ****$p < 0.0001$, ns: not statistically significant. LLC, Lewis lung cancer cells; PD-L1, programmed cell death-ligand 1

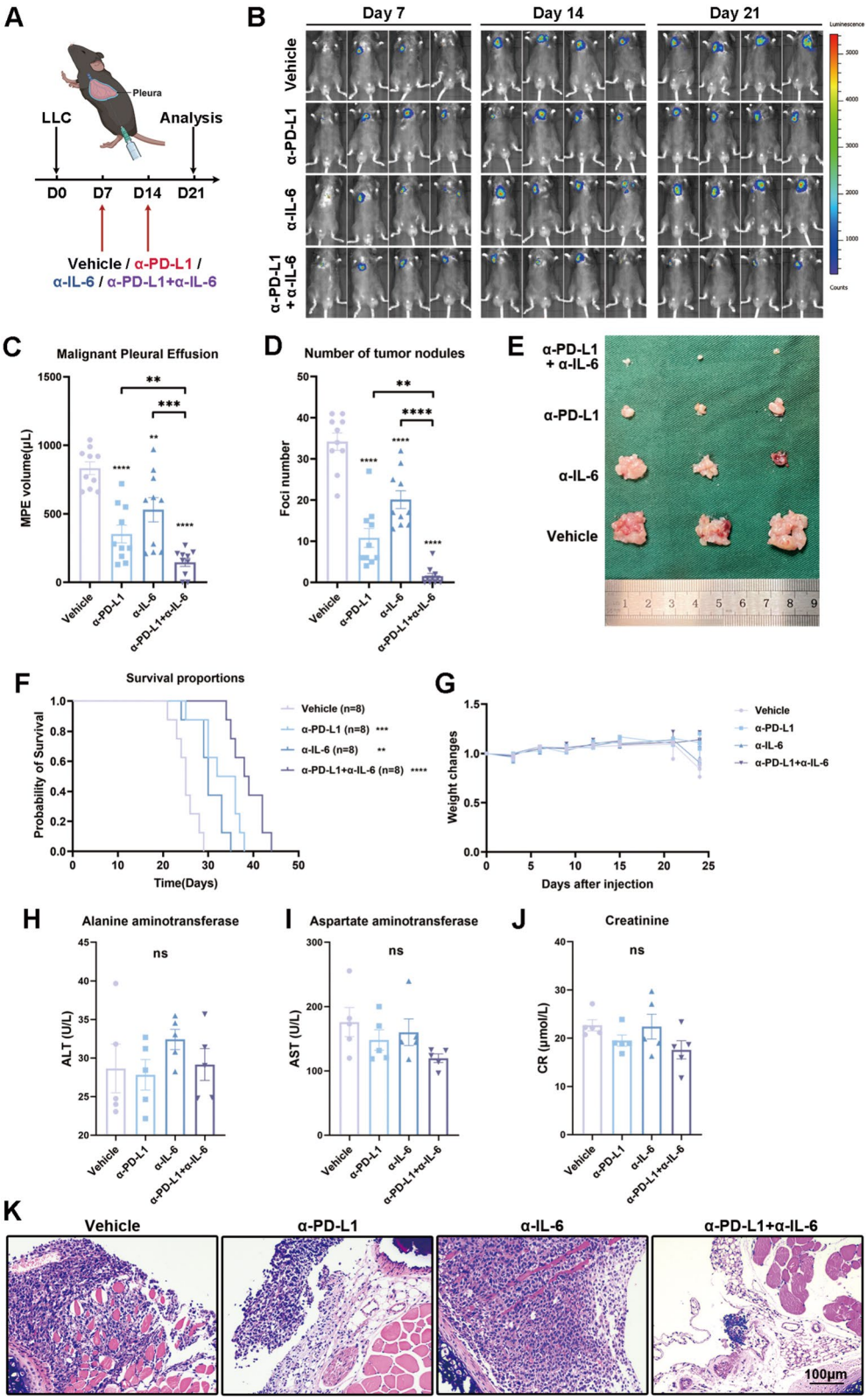

Fig. 1 (See legend on previous page.)

complementary deoxyribonucleic acid (cDNA) using the NEBNext Ultra RNA Library Prep Kit for Illumina (New England Biolabs). After that, cDNA underwent simple polymerase chain reaction (PCR) amplification before sequencing on an Illumina NovaSeq 6000 platform by Gene Denovo Biotechnology Co. Sequencing data showing a fold change > 2 and FDR < 0.05 were considered differentially expressed.

Western blotting

Mouse tumor nodules and cells with indicated treatment were collected and lysed for 30 min with radioimmunoprecipitation assay (RIPA) buffer (Servicebio, Wuhan, China) containing protease and phosphatase inhibitor cocktail (Beyotime, Shanghai, China) on ice. After centrifugation, the supernatant was gathered. The protein concentration was qualified using the bicinchoninic acid (BCA) protein assay kit (ThermoFisher Scientific, USA) and placed in a metal bath mixed with 1× loading buffer in equal amounts at 100 °C for 10 min. Proteins were separated by sodium dodecyl sulfate–polyacrylamide gel electrophoresis (SDS-PAGE) and moved onto polyvinylidene difluoride (PVDF) membranes (Merck, German). After being blocked with a solution like 5% BSA or 5% skim milk, the membranes were incubated with the following primary antibodies at 4 ℃ overnight: PD-L1 (ab271042, Abcam, 1:1000), STAT3 (#9139, CST, 1:2000), p-STAT3 (Tyr705, #9145, CST, 1:2000), Fibronectin 1 (FN1, #72026, CST,1:1000), collagen type I alpha 1 (COL1A1, #72026, CST, 1:1000), α-SMA (ab124964, Abcam, 1:50,000), glyceraldehyde-3-phosphate dehydrogenase (GAPDH, #60004-1-Ig, Proteintech, 1:100,000), β-actin (#66009-1-Ig, Proteintech, 1:50,000) and β-Tubulin (#66240-1-Ig, Proteintech, 1:100,000). After washing, they were incubated with HRP-conjugated secondary antibodies and visualized by a chemiluminescent analysis system for analysis.

qPCR

Total RNA was isolated from harvested tumor tissue and cells using TRIzol, following which cDNA was generated using the HiScript III RT SuperMix for qPCR (Vazyme, R323, Nanjing, China). Quantitative RT-qPCR was performed in duplicates using the ChamQ SYBR Color qPCR Master Mix (Vazyme, Q421, Nanjing, China) on the Quantagene q225 real-time PCR system (Kubo Technology, Beijing, China). Relative expression levels were calculated using the 2^-ΔΔCt method. The primer sequences in this assay are listed in Supplementary Table 4.

Statistical analysis

All experiments were repeated at least in triplicate, and the data were summarized as the mean ± standard error of the mean (SEM). Prism V.9 (GraphPad Software) was used to perform statistical analysis. Statistical significance was confirmed using a two-tailed Student's t-test and one-way analysis of variance. Survival analysis was calculated by the Kaplan–Meier method and executed using the log-rank test among groups. *P* values < 0.05 were set to indicate significance and indicated as follows: $^{*}p < 0.05$, $^{**}p < 0.01$, $^{***}p < 0.001$ and $^{****}p < 0.0001$.

Results

Elevated IL-6 levels in MPE of lung cancer patients correlate with PD-L1 expression

A total of 26 lung cancer patients were included in this study, comprising 18 males (69.2%) and 8 females (30.8%) with a median age of 56 years (Supplementary Table 1). Among these, 24 patients (92.3%) were diagnosed with lung adenocarcinoma (LUAD), one (3.8%) with lung squamous cell carcinoma (LUSC), and one (3.8%) with small cell lung cancer (SCLC). Analysis revealed that IL-6 concentrations were significantly higher in MPE compared with serum from the same patients (Supplementary Fig. 2A), indicating a tissue-specific accumulation of IL-6 in the pleural cavity. Using TIMER2.0 (http://timer.cistrome.org/), a positive correlation was identified between IL-6 and PD-L1 expression in 1,011 NSCLC patients from The Cancer Genome Atlas (TCGA; 501 LUSC and 510 LUAD; Supplementary Figs. 2B-C).

(See figure on next page.)

Fig. 2 IL-6 inhibition and PD-L1 blockade alleviates immunosuppression in MPE. **A** Representative flow cytometry images of $CD8^+$ T cells ($CD45^+CD3^+CD8^+$) and $CD4^+$ T cells ($CD45^+CD3^+CD4^+$) in MPE mice tumor nodules. The percentage of **B** $CD8^+$ T cells and **C** $CD4^+$ T cells in MPE mice tumor nodules were quantified by flow cytometry. The percentage of **D** IFN-γ^+ $CD8^+$ T cells ($CD45^+CD3^+CD8^+$IFN-γ^+) and **E** Granzyme B^+ $CD8^+$ T cells ($CD45^+CD3^+CD8^+$Granzyme B^+) in tumor nodules were evaluated by flow cytometry. **F** The percentage of $CD8^+$ Tem ($CD45^+CD3^+CD8^+CD44^+CD62L^-$), $CD8^+$ Tcm ($CD45^+CD3^+CD8^+CD44^+CD62L^+$) and $CD8^+$ naïve T cells ($CD45^+CD3^+CD8^+CD44^-CD62L^+$) in MPE mice tumor nodules were quantified by flow cytometry. **G** The percentage of $CD4^+$ Tem ($CD45^+CD3^+CD4^+CD44^+CD62L^-$), $CD4^+$ Tcm ($CD45^+CD3^+CD4^+CD44^+CD62L^+$) and $CD4^+$ naïve T cells ($CD45^+CD3^+CD4^+CD44^-CD62L.^+$) in MPE mice tumor nodules were quantified by flow cytometry. **H** Representative images of IHC staining of CD8, CD4, FOXP3, and F4/80 in MPE mice tumor nodules. Scale bar = 100 μm. All experiments were performed with ≥ 3 biological replicates. $^{*}p < 0.05$, $^{**}p < 0.01$, $^{***}p < 0.001$, $^{****}p < 0.0001$, ns: not statistically significant. Tem, effector memory T cells; Tcm, central memory T cells; FOXP3, forkhead box protein 3

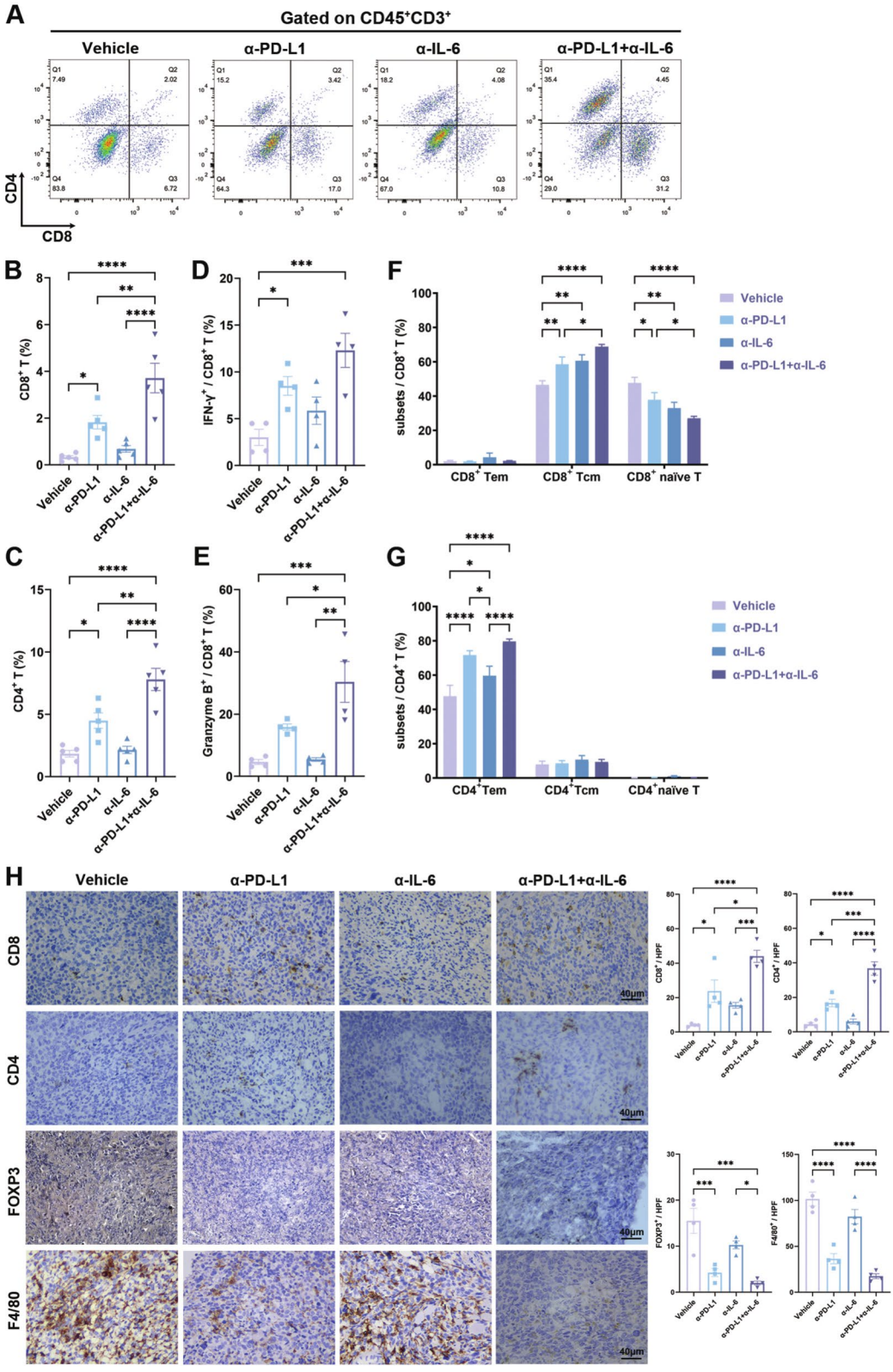

Fig. 2 (See legend on previous page.)

Furthermore, survival analysis using the Gene Expression Profiling Interactive Analysis (GEPIA) 2 database (http://gepia2.cancer-pku.cn/) database demonstrated that elevated IL-6 levels were associated with poorer survival rates in LUAD and LUSC patients (Supplementary Fig. 2D). These findings highlight the significant role of IL-6 in MPE and suggest its potential involvement in modulating immune escape mechanisms, providing a rationale for exploring combined IL-6 and PD-L1 blockade in MPE treatment.

Intrapleural dual blockade of IL-6 and PD-L1 alleviates immunosuppressive TME and controls MPE effectively in the mouse model

Anti-IL-6 mAb and anti-PD-L1 mAb were administered individually and in combination via intrapleural injection in the MPE mouse model to explore potential synergistic effects (Fig. 1A). The combination therapy group showed a significantly reduced MPE volume compared to the vehicle control group and either monotherapy group (Fig. 1B-C). This reduction suggests a potential synergistic effect of IL-6 inhibition and PD-L1 blockade in controlling pleural effusion. Moreover, the number of tumor nodules in the combination therapy group was notably fewer than that in the monotherapy or vehicle control groups, indicating a reduced tumor burden (Fig. 1D-E). The synergistic effects of IL-6 inhibitor and PD-L1 blockade effectively extended survival time (vehicle: 25 days, α-PD-L1: 34 days, α-IL-6: 30 days, combination therapy: 38.5 days) (Fig. 1F). Although weight loss was observed in all groups during advanced disease stages, the differences between groups were not statistically significant (Fig. 1G). No significant systemic toxicity was observed, as indicated by stable levels of creatinine (Cre), alanine aminotransferase (ALT), and aspartate aminotransferase (AST) across all groups, further supporting the tolerability of the intrapleural treatments (Fig. 1H-J). H&E staining of pleural tissue sections demonstrated that the severity of tumor invasion into pleural tissues was markedly reduced in the combination therapy group compared to the vehicle control and monotherapy groups (Fig. 1K). This reduced invasion not only highlights the efficacy of the combined therapy in limiting tumor growth but also suggests its potential role in mitigating tissue damage and local spread.

Analysis of tumor nodules in the MPE mouse model revealed significant changes in immune cell populations within the TME following combined therapy. $CD8^+$ and $CD4^+$ T cell infiltration levels were markedly increased in the combined therapy group compared to other groups (Fig. 2A-C). We further examined the functional activity of $CD8^+$ T cells by assessing IFN-γ and Granzyme B expression. Although overall $CD8^+$ T cell infiltration was limited, the combination therapy group showed a consistent trend toward higher proportions of IFN-γ^+ and Granzyme B^+ $CD8^+$ T cells, indicating enhanced cytotoxic function (Fig. 2D-E). Additional analysis showed that $CD8^+$ T cells predominantly transitioned to a central memory (Tcm) phenotype, accompanied by a reduction in naïve $CD8^+$ T cells (Fig. 2F). Similarly, $CD4^+$ T cells primarily shifted to an effector memory (Tem) phenotype, with their numbers notably elevated (Fig. 2G). These changes in T cell populations were accompanied by alterations in immunosuppressive components of the TME, including reductions in regulatory T cells (Tregs) and macrophages (Supplementary Figs. 3A-B). No significant differences were observed in the proportions of NK cells, NKT cells, monocytes, PMN-MDSCs, M-MDSCs, or neutrophils across the experimental groups (Supplementary Figs. 3C-E). IHC analysis corroborated these findings, showing increased $CD8^+$ and $CD4^+$ T cell infiltration and a reduction in Tregs and macrophages in the combined therapy group (Fig. 2H). These results suggest that IL-6 inhibition reduces MPE progression, alleviates immunosuppression in the TME, and enhances the potential efficacy of ICB therapy.

CAFs mediate the efficacy of combination therapy as revealed by RNA-seq analysis

To explore the synergistic effects of IL-6 inhibition and PD-L1 blockade, RNA sequencing (RNA-seq) was

(See figure on next page.)

Fig. 3 IL-6 inhibitor and PD-L1 blockade synergistically counteract tumorigenesis by mediating CAFs. **A** Transcriptomic sequencing and immune deconvolution analysis were used to identify significant changes in specific immune cell populations within the TME of pleural tissue with tumor nodules. **B** Schematic representation of the establishment of the MPE mouse model with or without NIH/3T3, and the treatment protocol with the vehicle solution, and anti-IL-6 mAb combined with anti-PD-L1 mAb. The MPE mice were randomly assigned to three groups. Created with BioRender. **C** Western blot analysis of α-SMA expression in NIH/3T3 co-cultured LLC at different ratios. GAPDH was used as the equal loading control. **D** Representative in vivo bioluminescence images of the growth of mice MPE. **E** Tumor nodule numbers and **F** MPE volume were observed. **G** Representative images of tumors nodules of the MPE mice. **H** A heatmap represented the differentially expressed genes related to CAFs. **I** KEGG pathway enrichment of the differentially expressed mRNA between the combined therapy group and the PD-L1 blockade group. All experiments were performed with ≥ 3 biological replicates. *$P < 0.05$, ***$p < 0.001$, ***$p < 0.001$, ****$p < 0.0001$, ns: not statistically significant. V, mice treated with the vehicle solution; L, mice treated with anti-IL-6 antibody; P, mice treated with anti-PD-L1 antibody; PL, mice treated with anti-IL-6 antibody and anti-PD-L1 antibody; KEGG, Kyoto Encyclopedia of Genes and Genomes

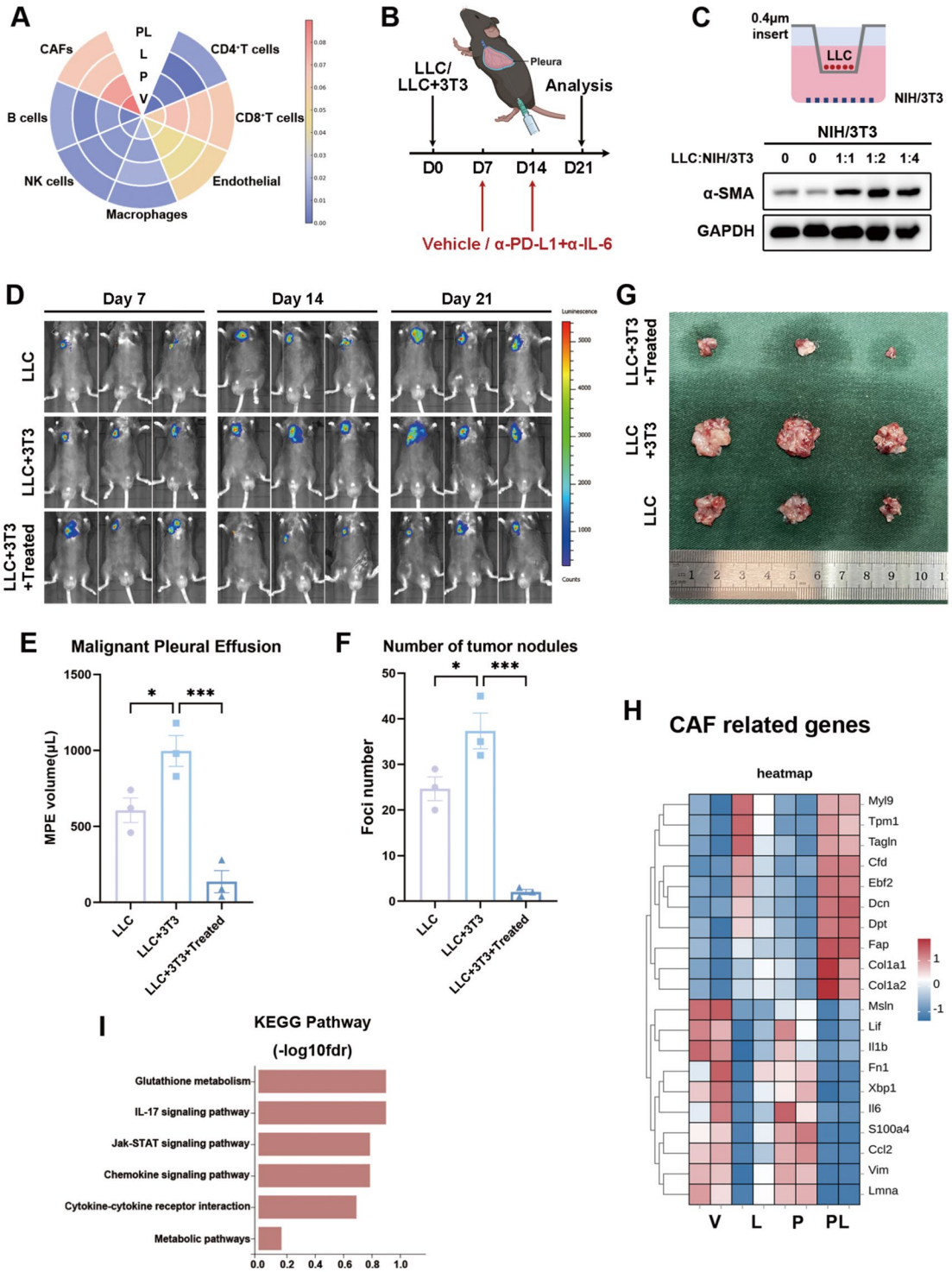

Fig. 3 (See legend on previous page.)

performed on pleural tissues containing tumor nodules from the MPE mouse model. Immune deconvolution using the Estimating the Proportion of Immune and Cancer cells (EPIC) method identified CAFs as the most significantly altered cell type among the experimental groups (Fig. 3A). TIMER2.0 analysis of lung cancer tissues further revealed a strong association between IL-6 and CAF infiltration, particularly in LUAD

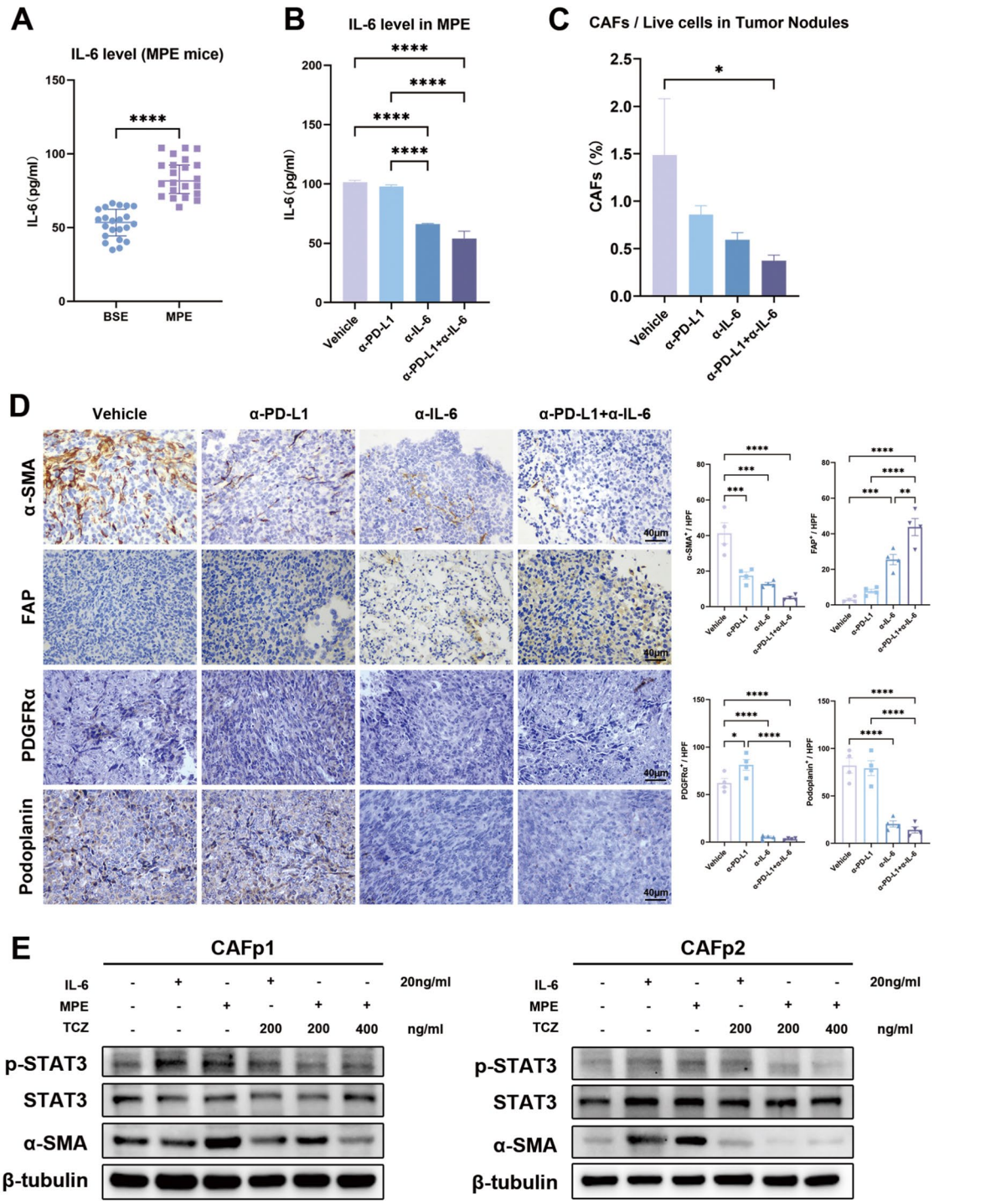

Fig. 4 IL-6 increased CAF infiltration in the MPE mouse model. Comparison of IL-6 levels in mice MPE **A** with serum and **B** between groups. **C** The percentage of the overall CAFs ($CD45^{-}CD90^{+}$) in mice tumor nodules were quantified by flow cytometry. **D** Representative images of IHC staining of α-SMA, PDGFRα, podoplanin, and FAP in MPE mice tumor nodules. Scale bar = 40 μm. **E** Western blot analysis of p-STAT3, STAT3, and α-SMA expression in CAFs treated with IL-6, MPE, MPE and tocilizumab. β-tubulin was used as the equal loading control. All experiments were performed with ≥ 3 biological replicates. *$p < 0.05$, **$p < 0.01$, ***$p < 0.001$, ****$p < 0.0001$, ns: not statistically significant. BSE: blood serum; MPE: malignant pleural effusion; FAP, fibroblast activation protein-α; α-SMA, α-smooth muscle actin; PDGFRα, platelet derived growth factor receptor α; CAFp1, CAFs isolated from patient 1; CAFp2, CAFs isolated from patient 2; TCZ, tocilizumab

(Supplementary Figs. 1E-F). $CD8^+$ T cells negatively correlated with IL-6 expression, while macrophages showed a positive correlation (Supplementary Fig. 1G-H). To validate the role of CAFs, an MPE mouse model was established by co-injecting NIH/3T3 fibroblasts and LLC tumor cells [35], with the experimental design and treatment protocol illustrated in Fig. 3B. NIH/3T3 cells were confirmed to acquire a CAF phenotype, characterized by α-SMA overexpression, upon co-culture with LLC cells (Fig. 3C). Mice co-injected with NIH/3T3 and LLC cells exhibited increased MPE volume and tumor nodule formation, which were significantly reduced by IL-6 inhibitor and PD-L1 blockade treatment (Fig. 3D-G).

Further analysis of the RNA-seq data revealed distinct expression patterns of CAF-related markers among the experimental groups. A heatmap visualization of these genes showed two distinct clusters: genes highly expressed in the vehicle and PD-L1 blockade groups were downregulated in the IL-6 inhibitor and combination therapy groups, while another cluster showed the opposite trend (Fig. 3H). These distinct expression patterns suggest heterogeneity in CAF populations, which may have differential roles within the TME. Kyoto Encyclopedia of Genes and Genomes (KEGG) pathway analysis comparing the combination therapy and PD-L1 blockade groups revealed enriched pathways, including glutathione metabolism, IL-17 signaling, and JAK-STAT signaling pathways, which may contribute to the observed changes in the TME (Fig. 3I). These findings prompted us to further investigate how IL-6 modulates CAF subtypes and their pro-inflammatory roles via STAT3 signaling.

IL-6 enhances CAF infiltration through the IL-6/STAT3 pathways

IL-6 expression was significantly higher in MPE compared to serum in the mouse model used in this study, consistent with findings in human MPE (Fig. 4A). Within the mouse model, IL-6 remained highly expressed in both the vehicle and PD-L1 blockade groups (Fig. 4B). Flow cytometry analysis revealed a reduction in the overall CAF population in the combined therapy group, while IHC analysis showed decreased expression of CAF-related proteins (Fig. 4C). These findings suggest that combination therapy may alter the characteristics of CAF subpopulations within the TME.

Given the reduction in CAF-related proteins and the known role of IL-6 in regulating CAF-associated markers, we further explored the role of IL-6 in influencing CAF-related changes in vitro. To this end, CAFs and NFs were isolated from tumor tissues and adjacent normal tissues of lung cancer patients, with CAFp1 and CAFp2 derived from two different patients. These fibroblast populations were identified by markers such as FN1, COL1A1 and α-SMA (Supplementary Figs. 4A-B). MPE was shown to activate NFs into CAFs in vitro (Supplementary Figs. 4C-D), while IL-6 alone failed to upregulate α-SMA in NFs (Supplementary Fig. 4C). However, IL-6 in MPE activated CAFs through the IL-6/STAT3 signaling pathway, as demonstrated by the inhibitory effect of tocilizumab (an anti-IL-6 receptor antibody) on MPE-induced CAF activation (Fig. 4E). These findings suggest that IL-6 primarily sustains the activity of already activated CAFs, potentially maintaining their pro-tumorigenic properties through the IL-6/STAT3 pathway.

IL-6 shifts CAF subtypes and suppresses iCAFs' pro-inflammatory role

To investigate CAF subtypes in the MPE mouse model, iCAFs, myCAFs, and antigen-presenting CAFs (apCAFs) were identified using Ly6C and MHCII markers [38–40] (Fig. 5A). iCAFs were the predominant subtype in the vehicle group (Fig. 5B), whereas myCAFs dominated in the combination therapy group treated with IL-6 inhibitor and anti-PD-L1 antibodies (Fig. 5C). ApCAFs showed a slight increase in the combination therapy group (Fig. 5D). Multiplex immunofluorescence demonstrated that IL-6 expression was significantly reduced in the combination therapy group (Fig. 5E). Further analysis in an MPE mouse model established by co-injecting CAFs and applying combination therapy revealed that, despite a reduced abundance of iCAFs, the expression of α-SMA, a myCAF marker, was relatively higher.

In pleural tumor nodules of MPE mice treated with anti-PD-L1 and -IL-6 antibody, the expression levels of iCAF-enriched genes, including *Il6*, *Pdgfra*, and *Lif*, were significantly reduced (Fig. 6A). To further

(See figure on next page.)

Fig. 5 IL-6 regulates CAFs and their subtype alterations to promote tumor growth. **A** Representative flow cytometry images of iCAFs ($CD45^-CD90^+Ly6C^+MHCII^-$), myCAFs ($CD45^-CD90^+Ly6C^-MHCII^-$) and apCAFs ($CD45^-CD90^+Ly6C^-MHCII^+$) in MPE mice tumor nodules. The percentage of **B** iCAFs, **C** myCAFs and **D** apCAFs in mice tumor nodules were quantified by flow cytometry. **E** Representative images of multiplex immunofluorescence of iCAFs (marked by PDGFRα and IL-6) in MPE mice tumor nodules. Scale bar = 100 μm. All experiments were performed with ≥ 3 biological replicates. $^*p < 0.05$, $^{**}p < 0.01$, $^{***}p < 0.001$, ns: not statistically significant. Ly6C, lymphocyte antigen 6 family member C; MHC, major histocompatibility complex; FAP, fibroblast activation protein-α; α-SMA, α-smooth muscle actin; PDGFRα, platelet derived growth factor receptor α; iCAF, inflammatory CAF; myCAF, myofibroblastic CAF; apCAF, antigen-presenting CAF

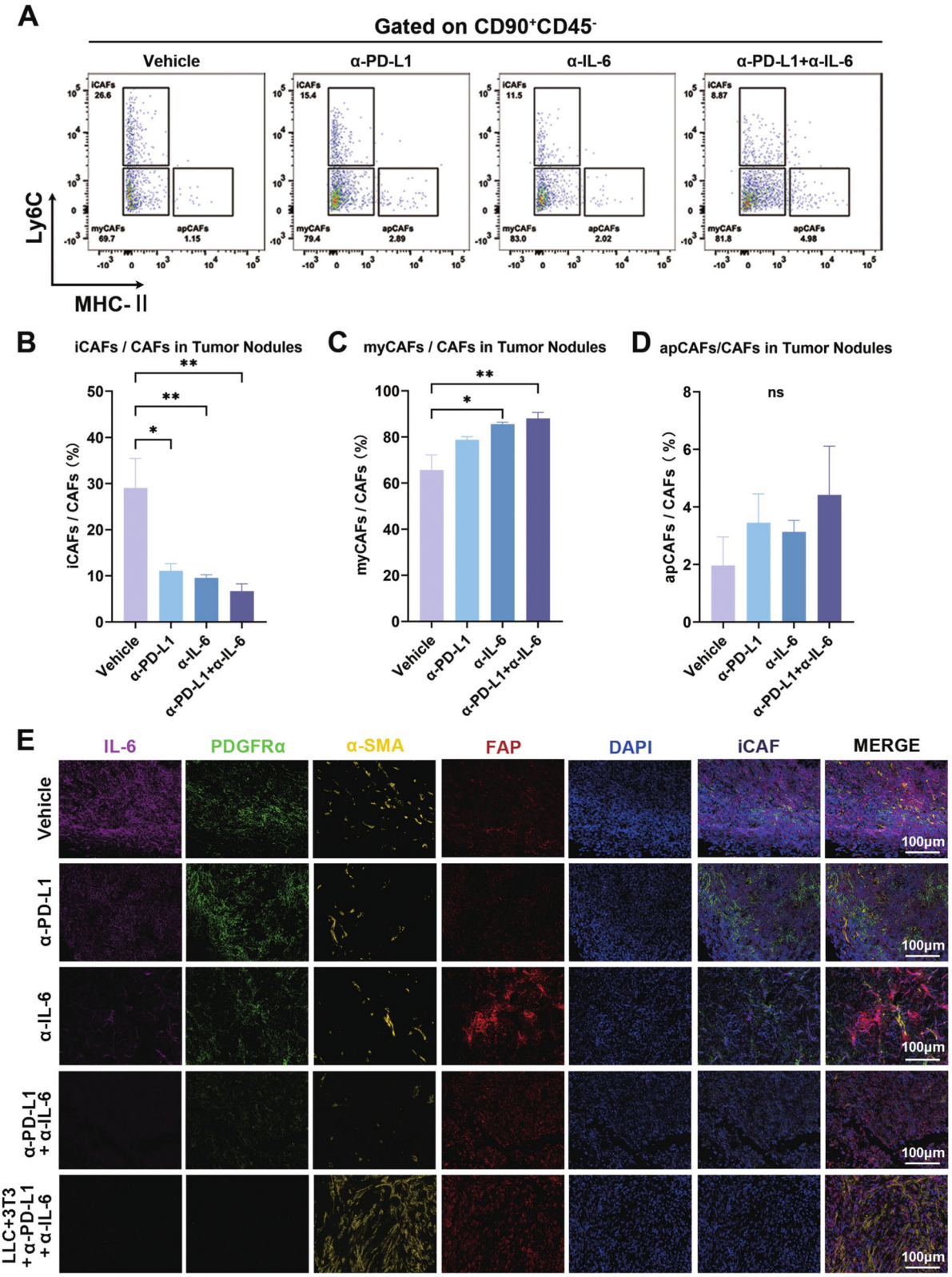

Fig. 5 (See legend on previous page.)

explore CAF subtypes, CAFs and PBMCs were co-cultured with MPE to simulate the immune microenvironment using an indirect transwell system (Fig. 6B). This approach allowed us to specifically assess the immunoregulatory effects of iCAF-secreted IL-6. Flow cytometry revealed an increased proportion of iCAFs following MPE treatment, which was reversed by tocilizumab, while myCAFs exhibited an opposite trend (Fig. 6C-D). These observations prompted further investigation into the relationship between IL-6 signaling and the regulation of iCAFs. IL-6 levels in the culture medium were elevated with MPE treatment but notably reduced by tocilizumab, indicating its effectiveness in reducing IL-6 production (Fig. 6E). MPE treatment also induced the expression of iCAF-enriched genes, including *IL6*, *PDGFRA*, and *LIF*, with *IL6* showing the highest induction. Tocilizumab significantly reduced the expression of these genes (Fig. 6F). A broader PCR array further confirmed *IL6* upregulation in MPE-conditioned CAFs, which was reduced by tocilizumab (Supplementary Fig. 5). These findings suggest that iCAFs play a pro-inflammatory role through IL-6 secretion, which may contribute to tumor progression in the MPE microenvironment. To directly assess how IL-6-producing CAFs affect immune killing, we designed a transwell-based indirect co-culture assay (Supplementary Fig. 6A). Lactate dehydrogenase (LDH) cytotoxicity assays showed that PBMC-mediated tumor killing was reduced in the presence of MPE, and this immunosuppressive effect was alleviated by tocilizumab (Supplementary Fig. 6B). These findings provide functional support for the immunosuppressive role of IL-6-producing CAFs in the MPE microenvironment.

IL-6 mediates PD-L1 upregulation via STAT3 activation in CAF-tumor interactions

Supplementary Figs. 1B-C revealed a positive correlation between PD-L1 and IL-6 expression in tumors, suggesting a potential regulatory link. RNA-seq analysis enriched the JAK/STAT signaling pathway (Fig. 3I), which is activated by IL-6, pointing to its possible role in PD-L1 regulation. Western blot analysis demonstrated that IL-6 and MPE treatment significantly increased PD-L1 expression and STAT3 phosphorylation in A549 cells, while tocilizumab and S3I-201 (a STAT3 inhibitor) both blocked these effects (Fig. 7A-B). In the MPE mouse model, combination therapy further reduced PD-L1 expression in tumor nodules, accompanied by decreased IL-6 and p-STAT3 levels (Fig. 7C-E), supporting the involvement of the IL-6/STAT3 pathway. To explore whether CAFs contribute to PD-L1 regulation via IL-6 secretion, A549 cells were co-cultured with CAFs, with or without tocilizumab (Fig. 7F). IL-6 levels in the co-culture medium increased significantly in untreated conditions but were markedly reduced with tocilizumab (Supplementary Fig. 7). Consistently, PD-L1 expression in A549 cells decreased after tocilizumab treatment, further implicating the IL-6/STAT3 axis in this interaction (Fig. 7G). These findings suggest that CAF-derived IL-6 promotes PD-L1 upregulation in tumors, providing a mechanistic basis for the observed efficacy of IL-6 and PD-L1 blockade in MPE treatment.

In conclusion, this study highlights the critical role of IL-6 in promoting tumor progression and immune evasion in MPE by regulating tumor PD-L1 expression through the IL-6/STAT3 pathway and modulating CAF subtypes, particularly iCAFs. Combination therapy targeting IL-6 and PD-L1 effectively reduced tumor burden, alleviated immunosuppression, and enhanced T cell infiltration in the MPE microenvironment. These findings provide a strong rationale for the dual blockade of IL-6 and PD-L1 as a promising therapeutic strategy for MPE.

Discussion

This study provides novel insights into the mechanisms driving immune suppression and tumor progression in lung cancer-associated MPE. We demonstrated that elevated IL-6 levels correlate with increased PD-L1 expression in MPE and are associated with poorer survival in lung cancer patients. Mechanistically, IL-6 regulates PD-L1 expression via the IL-6/STAT3 signaling pathway, promoting immune evasion. Importantly, our findings

(See figure on next page.)

Fig. 6 IL-6 in the MPE regulates CAFs and their subtype dynamics. **A** The mRNA expression of genes including *Fap, Pdpn, Pdgfra, Lif* and *Il6* of pleural tumor nodules of MPE mice treated with anti-PD-L1 and -IL-6 antibody, relative to *Actb*. **B** Schematic representation of the co-culture system of CAFs and PBMC. Created with BioRender. CAFs were serum-starved for 12 h and then treated with IL-6 and MPE, respectively, and tocilizumab was added to antagonize IL-6 in MPE. **C** The percentage of iCAFs ($CD90^+PDGFR\alpha^+HLA\text{-}DR^-$) and myCAFs ($CD90^+PDGFR\alpha^-HLA\text{-}DR^-$) of CAFp1, which was co-cultured with PBMC after MPE only and MPE and tocilizumab together, were quantified by flow cytometry. **D** The percentage of iCAFs ($CD90^+PDGFR\alpha^+HLA\text{-}DR^-$) and myCAFs ($CD90^+PDGFR\alpha^-HLA\text{-}DR^-$) of CAFp2, which was co-cultured with PBMC after MPE only and MPE and tocilizumab together, were quantified by flow cytometry. **F** IL-6 levels were assayed in the culture medium of CAFs treated with MPE only and MPE and tocilizumab. **G** The mRNA expression of genes such as *ACTA2, FAP, TAGLN, PDGFRA, IL6* and *LIF* of CAFs after co-culture with PBMC after MPE only and tocilizumab together, relative to *ACTB*. PBMC, peripheral blood mononuclear cell; CAFp1, CAFs isolated from patient 1; CAFp2, CAFs isolated from patient 2; TCZ, tocilizumab; NC, negative control

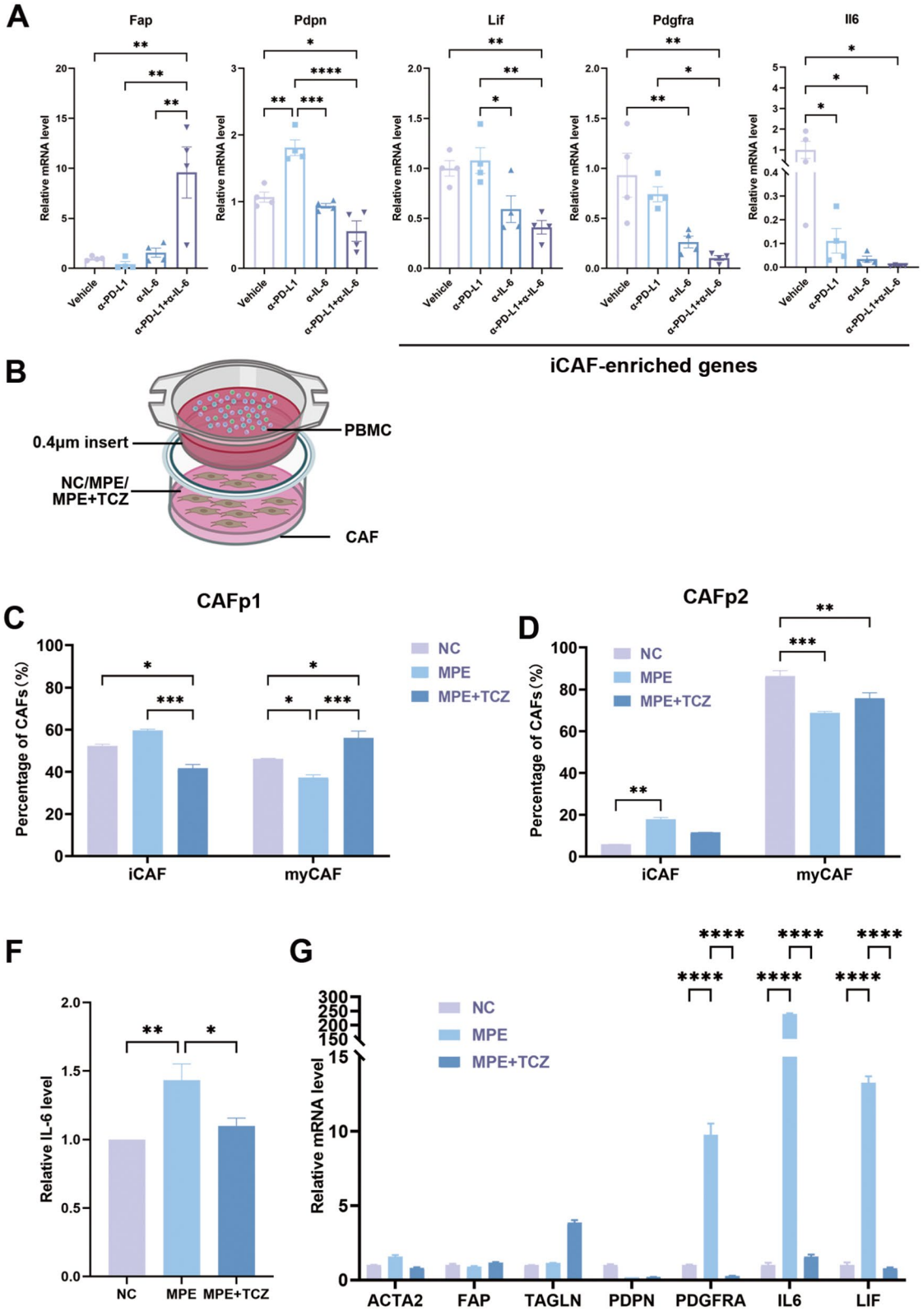

Fig. 6 (See legend on previous page.)

revealed that IL-6 also modulates CAF subtypes, particularly enhancing iCAFs that secrete high levels of IL-6 and drive an immunosuppressive TME. Combination therapy targeting IL-6 and PD-L1 significantly reduced tumor burden and reprogrammed the TME by reducing iCAFs and enhancing T cell infiltration. These findings provide preclinical evidence supporting dual IL-6 and PD-L1 blockade as a therapeutic strategy for lung cancer-associated MPE (Fig. 8).

Our previous study demonstrated that intrapleural injection of anti-PD-1 antibodies is effective and safe for treating lung cancer-associated MPE, but 22.2% (2/9) of patients still experienced early recurrence [8]. To investigate mechanisms of resistance to PD-1 therapy, we performed single-cell sequencing on paired MPE samples from relapsed patients (unpublished data). The analysis revealed a marked increase in fibroblast proportions in post-treatment MPE, suggesting that fibroblasts may play a role in resistance to ICB (Supplementary Fig. 8). This aligns with prior studies that identified CAF abundance as a key factor in MPE generation and progression [41]. Furthermore, the exploration of CAF heterogeneity has revealed distinct functional roles of CAF subtypes, particularly the pro-inflammatory iCAFs. Single-cell RNA sequencing studies across various tumors consistently demonstrate upregulation of the IL-6 signaling pathway in iCAFs, which is pivotal for cytokine secretion and immune modulation [32]. In line with these findings, our results further showed that IL-6 supports iCAF maintenance, as characterized by high expression of *IL6*, *PDGFRA*, and *LIF* [42, 43]. This forms a positive feedback loop that enhances immune suppression and cytokine secretion, contributing to MPE progression. Spatially resolved single-cell sequencing data further indicate that iCAFs exhibit high activity in immune-associated functions and interact with immune cells, especially $CD8^+$ T cells, to promote an immunosuppressive microenvironment [44]. Consistent with these observations, we found that IL-6-producing CAFs impaired immune responses both in vivo and in vitro, and this effect could be alleviated by IL-6 blockade.

We also observed a reduction in iCAF markers (IL-6 and PDGFRα) and an increase in FAP expression following dual IL-6 and PD-L1 blockade, suggesting a phenotypic shift from iCAF to myCAF-like populations. FAP is widely recognized as a key biomarker of CAFs and has been targeted in various anti-tumor strategies [26]. In the single-cell analysis of lung cancer, FAP^+ CAFs were found to possess collagen deposition, contraction, and adhesion activities, and classified as myCAFs [45]. However, the spatial positioning analysis of lung cancer revealed the irrelevance of FAP^+ CAFs to the distribution pattern of T cells in NSCLC [46]. Considering the context-dependent nature of myCAF identity and their heterogeneous roles across tumor types, we cautiously interpreted this shift without assigning a definitive subtype label. CAF subtype classification in our study was primarily based on flow cytometry analysis. We did not extend molecular characterization of myCAFs, as in vivo validation was limited. Our investigation focused on iCAFs due to their established immunosuppressive function and their close association with IL-6 signaling. We speculate that in MPE, where CAFs are mainly distributed along the pleura rather than forming dense stromal barriers, iCAFs may play a more dominant role. Driving the shift of iCAFs toward myCAF-like phenotypes might reduce local immune suppression while promoting pleural fibrosis. However, this remains hypothetical and requires further study. These findings underscore the dynamic role of CAF subtypes and highlight the importance of CAF-targeted strategies to complement immune checkpoint therapies.

The IL-6/STAT3 pathway emerged as a critical mechanism linking IL-6 to immune checkpoint regulation in the context of lung cancer-associated MPE. Bulk RNA-seq and immune deconvolution analyses identified IL-6 as a central cytokine associated with tumorigenesis and fibrogenesis in MPE [47]. Our study further demonstrated that IL-6 and MPE treatment promoted STAT3 phosphorylation and PD-L1 expression in tumor cells, while tocilizumab and S3I-201 effectively blocked this

(See figure on next page.)

Fig. 7 IL-6 regulated tumor PD-L1 expression via the IL-6/STAT3 pathway. **A** Western blot analysis of p-STAT3, STAT3 and PD-L1 in A549 cells serum-starved for 12 h and then treated with IL-6, IL-6 and tocilizumab, IL-6 and S3I-201 (a STAT3 inhibitor). β-actin was used as the equal loading control. **B** Western blot analysis of p-STAT3, STAT3 and PD-L1 in A549 cells serum-starved for 12 h and then treated with MPE, MPE and tocilizumab, MPE and S3I-201. β-actin was used as the equal loading control. **C** Quantification of PD-L1 expression in tumor cells ($CD45^-CD90^-$) in MPE mice tumor nodules by MFI analysis through flow cytometry. **D** Western blot analysis of PD-L1 in mice tumor nodules. β-actin was used as the equal loading control. **E** Representative images of IHC staining of IL-6 and p-STAT3 in the MPE mice tumor nodules. Scale bar = 100 μm. **F** Schematic representation of the co-culture system of CAFs and A549. A549 was serum-starved for 12 h and then co-cultured with CAFs and tocilizumab. **G** Western blot analysis of p-STAT3, STAT3, and PD-L1 in A549 cells co-cultured with CAFs and treated with tocilizumab. β-actin was used as the equal loading control. All experiments were performed with ≥ 3 biological replicates. *$p < 0.05$, **$p < 0.01$, ***$p < 0.001$, ****$p < 0.0001$, ns: not statistically significant. MFI, mean fluorescence intensity; tPD-L1, tumor PD-L1; CAFp1, CAFs isolated from patient 1; CAFp2, CAFs isolated from patient 2; TCZ, tocilizumab

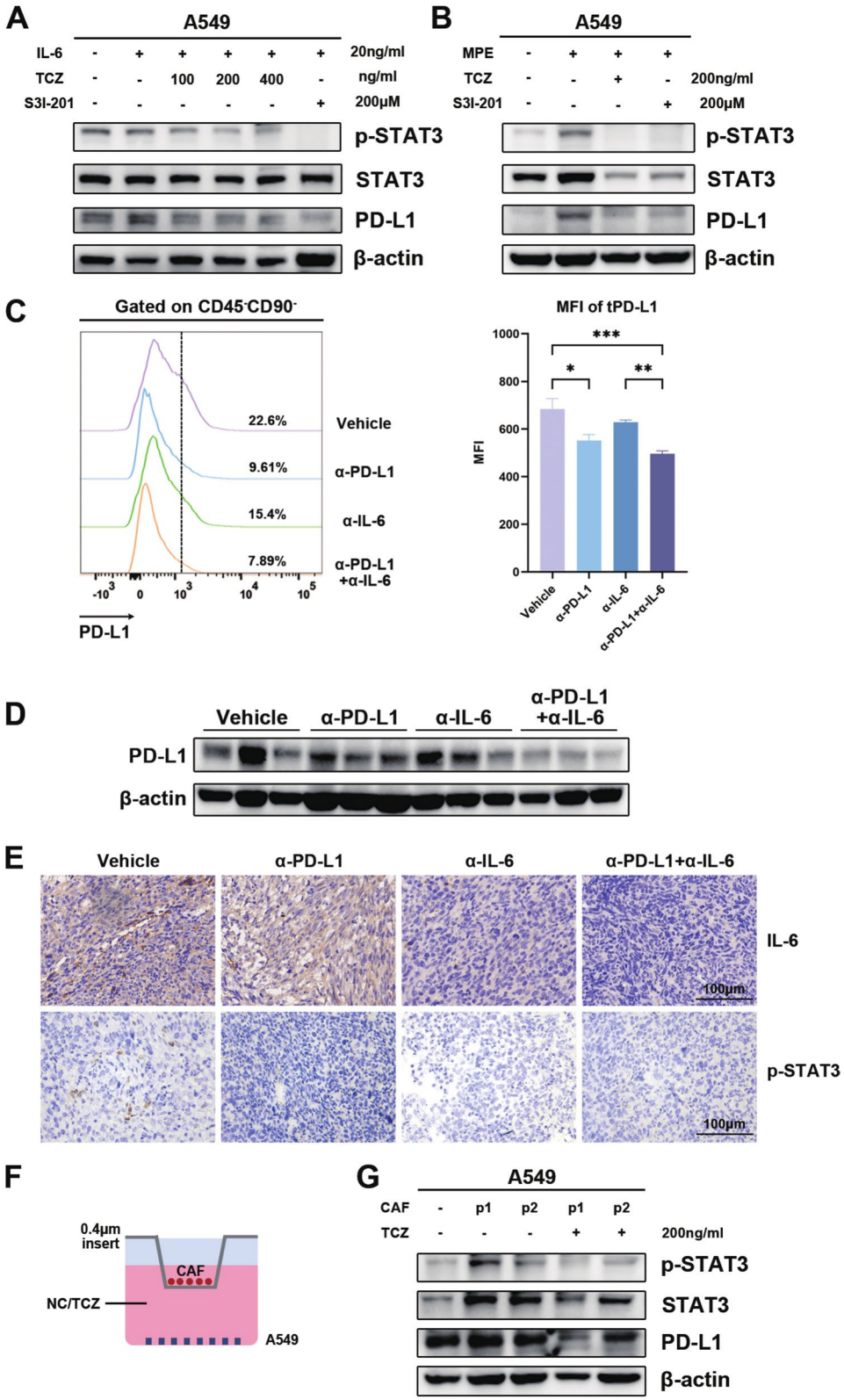

Fig. 7 (See legend on previous page.)

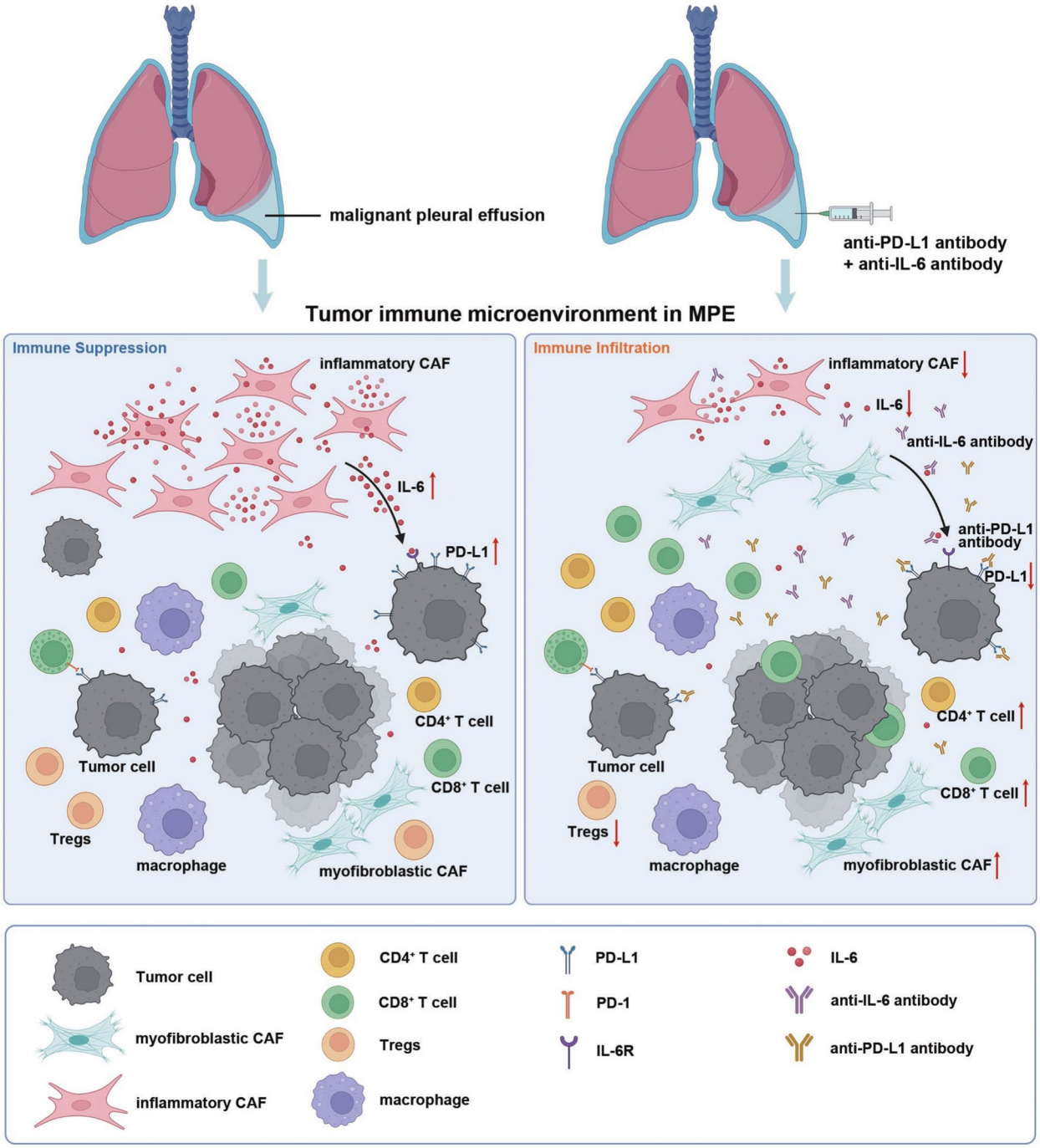

Fig. 8 A schematic diagram of the mechanism of IL-6 and PD-L1 dual blockade therapy for the intrapleural treatment of MPE. Elevated IL-6 in MPE contribute to an immunosuppressive microenvironment with low infiltration of $CD8^+$ T cells and high infiltration of iCAFs. IL-6 upregulates PD-L1 in tumor cells, thereby enhancing immunosuppression. Dual blockade of IL-6 and PD-L1 effectively reprograms the TME, reduces tumor burden, and enhances anti-tumor immunity. Created with BioRender

pathway. CAF-derived IL-6 upregulated PD-L1 expression in co-culture experiments, revealing a mechanistic link between stromal and immune components in driving immune suppression. These co-culture experiments were performed using an indirect transwell system, allowing us to assess the effect of CAF-derived IL-6 on tumor cells through soluble factors without direct cell–cell contact. These findings are consistent with previous

studies supporting the combination of anti-IL-6 therapy and immune checkpoint blockade across different tumor models [13]. Targeting CAFs has emerged as a promising approach to overcome immune resistance. IL-6/PD-L1 dual blockade may provide a more selective approach to modulate iCAFs with less structural disruption. Our findings support the potential of IL-6/PD-L1 dual blockade to reshape the local immune environment by reducing iCAFs and enhancing T cell activity. Detailed analysis of STAT3 downstream targets was not included in this study, as STAT3 remains clinically difficult to target [13, 48] and upstream blockade provides a more specific and translatable therapeutic strategy.

The therapeutic efficacy observed with dual IL-6 and PD-L1 blockade in this study suggests its potential for clinical application in managing lung cancer-associated MPE. This combination therapy not only reduced tumor burden but also alleviated local immunosuppression and enhanced T cell infiltration. Additionally, targeting iCAFs through IL-6 inhibition further underscores the potential for CAF-specific interventions to complement ICB. However, several limitations warrant consideration. The MPE mouse model, while effective in mimicking the localized immune suppression observed in human MPE, may not fully replicate the systemic immune responses in advanced lung cancer patients [49]. Although intrapleural therapy is commonly used in MPE, the combined local administration of IL-6 and PD-L1 dual blockade has not been evaluated in patients. CAF subtype classification and functional validation remain incomplete, particularly for myCAFs, which rely on mechanical and ECM signals difficult to replicate in vitro [50]. Thus, our analysis focused on iCAFs, which have more consistent immunosuppressive functions, and a clear association with IL-6 signaling. In our human sample analysis, the cohort size was limited by inclusion criteria and clinical availability. Limited pleural fluid cellularity also hindered marker-level validation of CAFs and PD-L1. To address these limitations, we are currently expanding MPE sample collection and conducting single-cell sequencing to characterize the immune-stromal landscape and guide biomarker-driven therapeutic strategies. In parallel, we are analyzing pleural metastasis tissues using spatial transcriptomics to support translational studies. These efforts are expected to provide a more comprehensive understanding of CAF heterogeneity and its immunomodulatory roles. Given the localized immunosuppressive nature of MPE, dual IL-6 and PD-L1 blockade may offer a promising therapeutic strategy. Clinical trials are required to further evaluate the feasibility and safety of this approach in MPE patients.

Conclusion

In conclusion, this study highlights the critical role of IL-6 in promoting tumor progression and immune evasion in MPE by regulating PD-L1 expression through the IL-6/STAT3 pathway and modulating CAF subtypes, particularly iCAFs. Combination therapy targeting IL-6 and PD-L1 effectively reduced tumor burden, alleviated immunosuppression, and enhanced T cell infiltration in the MPE microenvironment. These findings provide a strong rationale for the dual blockade of IL-6 and PD-L1 as a promising therapeutic strategy for MPE.

Abbreviations

MPE	Malignant pleural effusion
IL-6	Interleukin-6
TME	Tumor microenvironment
ICB	Immune checkpoint blockade
CAF	Cancer associated fibroblast
iCAF	Inflammatory CAF
myCAF	Myfibroblastic CAF
apCAF	Antigen-presenting CAFs
PD-L1	Programmed cell death-ligand 1
STAT	Signal transducer and activator of transcription
Tcm	Central memory T cell
Tem	Effector memory T cell
TAM	Tumor-associated macrophage
MDSC	Myeloid-derived suppressor cell
Tregs	Regulatory T cell
NK	Natural killer
PMC	Pleural mesothelial cell
ECM	Extracellular matrix
FAP	Fibroblast activation protein-α
α-SMA	α-Smooth muscle actin
PDGFRα	Platelet derived growth factor receptor α
MHC	Major histocompatibility complex
PBMC	Peripheral blood mononuclear cell
LUAD	Lung adenocarcinoma
LUSC	Lung squamous cell carcinoma

Supplementary Information

The online version contains supplementary material available at https://doi.org/10.1186/s12931-025-03263-0.

Supplementary Material 1.

Supplementary Material 2.

Acknowledgements

We would like to thank the laboratories of the Department of Diagnostic Radiology of Jinling Hospital (Affiliated Hospital of Medical School, Nanjing University) for providing the necessary equipment for this study. We also express gratitude to all the patients who participated in our study.

Authors' contributions

QC and XZ contributed equally. QC and TL wrote the manuscript, generated figures, designed experiments, performed experiments, and analyzed data; XZ, ZW, and JL performed experiments, provided resources, and edited the manuscript; YS, PZ, and TL supervised the study, provided resources, and edited the manuscript; WL and YJ performed experiments and edited the manuscript; XL, QX, SZ and XL verified data and edited the manuscript. TL accepted full responsibility for the work and the conduct of the study. All co-authors read, edited, and approved the manuscript.

Funding
This work was supported by grants from the National Natural Science Foundation of China (#82370096, #82200110), Noncommunicable Chronic Diseases-National Science and Technology Major Project (2024ZD0522800 to P Tian, 2024ZD0522806 to T Lv), and the Science and Technology Innovation Research Project of Jinling Hospital (#22LCYY-LH3).

Data availability
No datasets were generated or analysed during the current study.

Declarations

Ethics approval and consent to participate
The studies using human specimens were approved by the Ethical Committee and Institutional Review Board of the Jinling Hospital (#2021DZGZR-YBB-063). The participants provided their informed consent to participate in the study. All animal experiments were approved by the Ethical Committee and Institutional Review Board of the Jinling Hospital (#2021DZGKJDWLS-0089).

Consent for publication
Not applicable.

Competing interests
The authors declare no competing interests.

Author details
[1]Present Address: Department of Respiratory and Critical Care Medicine, Jinling Hospital, Affiliated Hospital of Medical School, Nanjing University, Nanjing, China. [2]Department of Respiratory and Critical Care Medicine, Nanjing Drum Tower Hospital, Affiliated Hospital of Medical School, Nanjing University, Nanjing, China. [3]Department of Respiratory and Critical Care Medicine, School of Medicine, Affiliated Jinling Hospital, Southeast University, Nanjing, China.

Received: 28 November 2024 Accepted: 29 April 2025
Published online: 10 May 2025

References

1. Zamboni MM, da Silva CT, Baretta R, Cunha ET, Cardoso GP. Important prognostic factors for survival in patients with malignant pleural effusion. BMC Pulm Med. 2015;28(15):29.
2. Antony VB, Loddenkemper R, Astoul P, Boutin C, Goldstraw P, Hott J, et al. Management of malignant pleural effusions. Eur Respir J. 2001;18(2):402–19.
3. Gonnelli F, Hassan W, Bonifazi M, Pinelli V, Bedawi EO, Porcel JM, et al. Malignant pleural effusion: current understanding and therapeutic approach. Respir Res. 2024;25(1):47.
4. Psallidas I, Kalomenidis I, Porcel JM, Robinson BW, Stathopoulos GT. Malignant pleural effusion: from bench to bedside. Eur Respir Rev. 2016;25(140):189–98.
5. Asciak R, Rahman NM. Malignant Pleural Effusion: From Diagnostics to Therapeutics. Clin Chest Med. 2018;39(1):181–93.
6. Murthy P, Ekeke CN, Russell KL, Butler SC, Wang Y, Luketich JD, et al. Making cold malignant pleural effusions hot: driving novel immunotherapies. Oncoimmunology. 2019;8(4):e1554969.
7. Antonia SJ, Villegas A, Daniel D, Vicente D, Murakami S, Hui R, et al. Overall Survival with Durvalumab after Chemoradiotherapy in Stage III NSCLC. N Engl J Med. 2018;379(24):2342–50.
8. Li X, Wu G, Chen C, Zhao Y, Zhu S, Song X, et al. Intrapleural Injection of Anti-PD1 Antibody: A Novel Management of Malignant Pleural Effusion. Front Immunol. 2021;13(12):760683.
9. Vesely MD, Zhang T, Chen L. Resistance Mechanisms to Anti-PD Cancer Immunotherapy. Annu Rev Immunol. 2022;26(40):45–74.
10. Principe N, Kidman J, Lake RA, Lesterhuis WJ, Nowak AK, McDonnell AM, et al. Malignant Pleural Effusions—A Window Into Local Anti-Tumor T Cell Immunity? Front Oncol. 2021;27:11.
11. Donnenberg AD, Luketich JD, Dhupar R, Donnenberg VS. Treatment of malignant pleural effusions: the case for localized immunotherapy. J Immunother Cancer. 2019;7(1):110.
12. Johnson DE, O'Keefe RA, Grandis JR. Targeting the IL-6/JAK/STAT3 signalling axis in cancer. Nat Rev Clin Oncol. 2018;15(4):234–48.
13. Soler MF, Abaurrea A, Azcoaga P, Araujo AM, Caffarel MM. New perspectives in cancer immunotherapy: targeting IL-6 cytokine family. J Immunother Cancer. 2023;11(11):e007530.
14. Nagasaki T, Hara M, Nakanishi H, Takahashi H, Sato M, Takeyama H. Interleukin-6 released by colon cancer-associated fibroblasts is critical for tumour angiogenesis: anti-interleukin-6 receptor antibody suppressed angiogenesis and inhibited tumour-stroma interaction. Br J Cancer. 2014;110(2):469–78.
15. Karakasheva TA, Lin EW, Tang Q, Qiao E, Waldron TJ, Soni M, et al. IL-6 Mediates Cross-Talk between Tumor Cells and Activated Fibroblasts in the Tumor Microenvironment. Cancer Res. 2018;78(17):4957–70.
16. Fujino S, Yokoyama A, Kohno N, Hiwada K. Interleukin 6 is an autocrine growth factor for normal human pleural mesothelial cells. Am J Respir Cell Mol Biol. 1996;14(6):508–15.
17. Choo YY, Sakai T, Komatsu S, Ikebe R, Jeffers A, Singh KP, et al. Calponin 1 contributes to myofibroblast differentiation of human pleural mesothelial cells. Am J Physiol Lung Cell Mol Physiol. 2022;322(3):L348–64.
18. Whitfield HJ, Berthelet J, Mangiola S, Bell C, Anderson RL, Pal B, et al. Single-cell RNA sequencing captures patient-level heterogeneity and associated molecular phenotypes in breast cancer pleural effusions. Clin Transl Med. 2023;13(9):e1356.
19. Liu C, Yang L, Xu H, Zheng S, Wang Z, Wang S, et al. Systematic analysis of IL-6 as a predictive biomarker and desensitizer of immunotherapy responses in patients with non-small cell lung cancer. BMC Med. 2022;13(20):187.
20. Liu H, Shen J, Lu K. IL-6 and PD-L1 blockade combination inhibits hepatocellular carcinoma cancer development in mouse model. Biochem Biophys Res Commun. 2017;486(2):239–44.
21. Mace TA, Shakya R, Pitarresi JR, Swanson B, McQuinn CW, Loftus S, et al. IL-6 and PD-L1 antibody blockade combination therapy reduces tumour progression in murine models of pancreatic cancer. Gut. 2018;67(2):320–32.
22. Tsukamoto H, Fujieda K, Miyashita A, Fukushima S, Ikeda T, Kubo Y, et al. Combined Blockade of IL6 and PD-1/PD-L1 Signaling Abrogates Mutual Regulation of Their Immunosuppressive Effects in the Tumor Microenvironment. Cancer Res. 2018;78(17):5011–22.
23. Huseni MA, Wang L, Klementowicz JE, Yuen K, Breart B, Orr C, et al. CD8+ T cell-intrinsic IL-6 signaling promotes resistance to anti-PD-L1 immunotherapy. Cell Rep Med. 2023;4(1):100878.
24. Shiga K, Hara M, Nagasaki T, Sato T, Takahashi H, Takeyama H. Cancer-Associated Fibroblasts: Their Characteristics and Their Roles in Tumor Growth. Cancers (Basel). 2015;7(4):2443–58.
25. Song L, Smith MA, Doshi P, Sasser K, Fulp W, Altiok S, et al. Antitumor efficacy of the anti-interleukin-6 (IL-6) antibody siltuximab in mouse xenograft models of lung cancer. J Thorac Oncol. 2014;9(7):974–82.
26. Zhang H, Yue X, Chen Z, Liu C, Wu W, Zhang N, et al. Define cancer-associated fibroblasts (CAFs) in the tumor microenvironment: new opportunities in cancer immunotherapy and advances in clinical trials. Mol Cancer. 2023;2(22):159.
27. Biffi G, Tuveson DA. Diversity and Biology of Cancer-Associated Fibroblasts. Physiol Rev. 2021;101(1):147–76.
28. Özdemir BC, Pentcheva-Hoang T, Carstens JL, Zheng X, Wu CC, Simpson TR, et al. Depletion of carcinoma-associated fibroblasts and fibrosis induces immunosuppression and accelerates pancreas cancer with reduced survival. Cancer Cell. 2014;25(6):719–34.
29. Bhattacharjee S, Hamberger F, Ravichandra A, Miller M, Nair A, Affo S, et al. Tumor restriction by type I collagen opposes tumor promoting effects of cancer-associated fibroblasts. J Clin Invest. 2021;131(11):e146987.
30. Chen Y, Kim J, Yang S, Wang H, Wu CJ, Sugimoto H, et al. Type I collagen deletion in αSMA+ myofibroblasts augments immune suppression and accelerates progression of pancreatic cancer. Cancer Cell. 2021;39(4):548-565.e6.
31. Biffi G, Oni TE, Spielman B, Hao Y, Elyada E, Park Y, et al. IL-1-induced JAK/STAT signaling is antagonized by TGF-β to shape CAF heterogeneity in pancreatic ductal adenocarcinoma. Cancer Discov. 2019;9(2):282–301.
32. Lavie D, Ben-Shmuel A, Erez N, Scherz-Shouval R. Cancer-associated fibroblasts in the single-cell era. Nat Cancer. 2022;3(7):793–807.
33. Tsoumakidou M. The advent of immune stimulating CAFs in cancer. Nat Rev Cancer. 2023;23(4):258–69.

34. Lakins MA, Ghorani E, Munir H, Martins CP, Shields JD. Cancer-associated fibroblasts induce antigen-specific deletion of CD8 + T Cells to protect tumour cells. Nat Commun. 2018;9(1):948.
35. Kato T, Noma K, Ohara T, Kashima H, Katsura Y, Sato H, et al. Cancer-Associated Fibroblasts Affect Intratumoral CD8+ and FoxP3+ T Cells Via IL6 in the Tumor Microenvironment. Clin Cancer Res. 2018;24(19):4820–33.
36. Nishiwaki N, Noma K, Ohara T, Kunitomo T, Kawasaki K, Akai M, et al. Overcoming cancer-associated fibroblast-induced immunosuppression by anti-interleukin-6 receptor antibody. Cancer Immunol Immunother. 2023;72(7):2029–44.
37. McAndrews KM, Chen Y, Darpolor JK, Zheng X, Yang S, Carstens JL, et al. Identification of Functional Heterogeneity of Carcinoma-Associated Fibroblasts with Distinct IL6-Mediated Therapy Resistance in Pancreatic Cancer. Cancer Discov. 2022;12(6):1580–97.
38. Schwörer S, Cimino FV, Ros M, Tsanov KM, Ng C, Lowe SW, et al. Hypoxia potentiates the inflammatory fibroblast phenotype promoted by pancreatic cancer cell-derived cytokines. Cancer Res. 2023;83(10):1596–610.
39. Liu T, Han C, Fang P, Ma Z, Wang X, Chen H, et al. Cancer-associated fibroblast-specific lncRNA LINC01614 enhances glutamine uptake in lung adenocarcinoma. J Hematol Oncol. 2022;8(15):141.
40. Elyada E, Bolisetty M, Laise P, Flynn WF, Courtois ET, Burkhart RA, et al. Cross-species single-cell analysis of pancreatic ductal adenocarcinoma reveals antigen-presenting cancer-associated fibroblasts. Cancer Discov. 2019;9(8):1102–23.
41. Ibrahim FM, Helal DS, Ali DA, Abd-Ellatif RN, Elkady AM, Sharshar R, et al. Prognostic role of annexin A2 and cancer-associated fibroblasts in advanced non-small cell lung cancer: Implication in epithelial-mesenchymal transition and gefitinib resistance. Pathol Res Pract. 2023;241:154293.
42. Guo T, Xu J. Cancer-associated fibroblasts: a versatile mediator in tumor progression, metastasis, and targeted therapy. Cancer Metastasis Rev. 2024;43(3):1095–116.
43. Cassier PA, Navaridas R, Bellina M, Rama N, Ducarouge B, Hernandez-Vargas H, et al. Netrin-1 blockade inhibits tumour growth and EMT features in endometrial cancer. Nature. 2023;620(7973):409–16.
44. Ma C, Yang C, Peng A, Sun T, Ji X, Mi J, et al. Pan-cancer spatially resolved single-cell analysis reveals the crosstalk between cancer-associated fibroblasts and tumor microenvironment. Mol Cancer. 2023;13(22):170.
45. Xiang H, Pan Y, Sze MA, Wlodarska M, Li L, van de Mark KA, et al. Single-Cell Analysis Identifies NOTCH3-Mediated Interactions between Stromal Cells That Promote Microenvironment Remodeling and Invasion in Lung Adenocarcinoma. Cancer Res. 2024;84(9):1410–25.
46. Grout JA, Sirven P, Leader AM, Maskey S, Hector E, Puisieux I, et al. Spatial positioning and matrix programs of cancer-associated fibroblasts promote T cell exclusion in human lung tumors. Cancer Discov. 2022;12(11):2606–25.
47. Bruschini S, Pallocca M, Sperandio E, D'Ambrosio L, Ascenzi F, De Vitis C, et al. Deconvolution of malignant pleural effusions immune landscape unravels a novel macrophage signature associated with worse clinical outcome in lung adenocarcinoma patients. J Immunother Cancer. 2022;10(5):e004239.
48. Berkley K, Zalejski J, Sharma A. Targeting STAT3 for Cancer Therapy: Focusing on Y705, S727, or Dual Inhibition? Cancers (Basel). 2025;17(5):755.
49. Zhang X, Wang X, Wen Y, Chen S, Zhou C, Wu F. Single-cell transcriptomics reveal metastatic CLDN4+ cancer cells underlying the recurrence of malignant pleural effusion in patients with advanced non-small-cell lung cancer. Clin Transl Med. 2024;14(4):e1649.
50. Lee JY, Chaudhuri O. Regulation of Breast Cancer Progression by Extracellular Matrix Mechanics: Insights from 3D Culture Models. ACS Biomater Sci Eng. 2018;4(2):302–13.

Publisher's Note

Springer Nature remains neutral with regard to jurisdictional claims in published maps and institutional affiliations.